THE ZWITTERION ISOMER OF ORTHOSILICIC ACID AND ITS ROLE IN NEUTRAL pH DIMERIZATION FROM DENSITY FUNCTIONAL THEORY

Mihali A. Felipe

Molecular Biophysics & Biochemistry
Yale University
New Haven CT 06511 USA
mihali.felipe@yale.edu

ABSTRACT

Using density functional theory, the plausible existence of the zwitterion isomer of orthosilicic acid is proposed to account for some of the properties of silica in water. Explicit hydration and explicit addition of salt are used in modeling the zwitterion and the dimerization reaction. Paths between orthosilicic acid, the zwitterion and the autoionization products are presented. The pK for the formation of the aqueous zwitterion species is calculated to be 7.8 and the activation energy for the dimerization reaction ranges from 14.3 kcal/mol to 16.9 kcal/mol.

1.0 Introduction

Orthosilicic acid is the most fundamental building block of dissolved silica, which are themselves among the most ubiquitous classes of compounds found in surface waters. A thorough understanding of the chemistry of orthosilicic acid is therefore vital to elucidate phenomena involving silica such as mineralization, nutrient bioavailability, and geothermal well

scaling. Unfortunately, although great effort has been expended in experiments and simulation, the dimerization reaction, which is one of the simplest of its reactions, is still not very well understood; the same can be said about the reverse reaction, or the hydrolysis of the dimer.

Studies on the reaction order are conflicting and are an indication that much is not known about the dynamics of silica in solution at the atomic scale. Studies at pH 4 by Alexander et al. (1954) showed third order kinetics in agreement with Goto (1956) who conducted work at pH 7 to 10. However, Rothbaum and Rohde (1979) found the oligomerization at pH 7 to 8 to be second order and Icopini et al. (2005) reported fourth order rates from pH 3 to 11. Gorrepati et al. (2010) found second order rates below pH 0. The activation energies from these studies vary from 3 kcal/mol (Rothbaum and Rohde, 1979), to 13.86 kcal/mol (Harrison and Loton, 1995), to 17 kcal/mol (Makrides et al., 1980).

The dependence of the kinetics on ionic activity, or alternatively cation concentration, is just as puzzling (Rimstidt, 2015). Sodium ion has been shown to decrease the reaction rate of silica condensation at early stages (Harrison and Loton, 1995) yet increase crystallization and growth at later stages (Burkett and Davis, 1995). Icopini et al. (2005) found an exponential increase in oligomerization rates with ionic activity. Gorrepatti et al (2010) found rates that varied with the salt added according to the following relationship: $AlCl_3$ > $CaCl_2$ > $MgCl_2$ > NaCl > CsCl > no salt. How these phenomena happen is unresolved. The complex relationships between rates and pH and ionic activity opens up the question of the existence of yet unidentified reactive species or class of species that favor neutral pH and high ionic activity.

Simulation has been providing immense insight understanding the dimerization process and discovering species that would not otherwise have been easily identified by experiment.

Simulation methods have grown in sophistication in parallel with the development of computing memory and processing power. The primary emphasis in the present study is on density functional theory methods (DFT) specifically, although other schemes that are in active development and application such as molecular dynamics (Iztova et al, 2020; Kirk et al., 2011; Jorge et al., 2009) and Monte Carlo (Martin et al., 2021; Zhang et al., 2012; Malani et al. 2010) have also been applied to investigate these mechanism. These other schemes are able to model chemical systems on the micro-scale that would not be practicable with DFT. However, the elucidation of chemical reactivity is still principally a question that is best handled on the atomic-scale by DFT and ab initio methods in general because of the changes in bonding, and therefore electronic structure, during the course of a reaction. At the same time, it is worth noting that there are methods that algorithmically combine the strengths of both ab initio and molecular dynamics aptly named ab initio molecular dynamics (Pavlova et al., 2013; Trinh et al., 2009; Car and Parinello, 1985).

The impetus of these simulations is to model the real system as closely as computationally practical, and to incorporate all physical influences on the reaction center. In this regard, the nascent ab initio work by Xiao and Lasaga (1996, 1994) on acid and base catalyzed hydrolysis of the dimer were attempts to draw silica solution chemistry from dry, gas-phase simulations. Subsequently, the utilization of implicit solvation improved the energy calculations taking into account long range effects that the solvent imparts on the reacting ensemble (Mora-Fonz and Catlow, 2007; Pelmenschikov et al., 1997; Tossel, 2005) without significant computational overhead. However, the explicit addition of water molecules revealed that favorable reaction paths may be starkly different from the dry, gas-phase simulations, even with implicit solvation included (Trinh et al., 2009; Heenan et al., 2020; Zhang et al., 2017) suggesting that long range

interactions have a less influential role on the mechanisms than short range electrostatics and, more specifically, than hydrogen bonding. These effects are predominantly due to the ease of formation of hydrogen bonds by water molecules, which lowers energies significantly (3-8 kcal mol^{-1}, Huš and Urbic, 2012), and the ability of water to form proton wires where hydrogens can concertedly move around and participate in the so-called Grotthus mechanism (van Grotthus, 1806; e.g., Liu et al., 2019). Furthermore, the hydroxides of H_4SiO_4 themselves have been shown to participate in mobilizing hydrogen through similar mechanism (Felipe et al., 2004) in aqueous environments.

It is interesting to note that studies on the neutral mechanism examine the dimerization primarily focusing on the reactivity of H_4SiO_4, and in particular relying on the nucleophilicity of hydroxide oxygens and the electro-positivity of the central silicon. For example, Trinh et al. (2006) arrived at a one-step dimerization mechanism where the hydroxide oxygen of one orthosilicic acid attacks the silicon of another directly. This had an activation energy of 30.4 kcal/mol. The energetics of these mechanisms were corroborated by later studies with modifications (Hu et al. 2013; Liu et al., 2019). However, as more studies come out, it becomes apparent that the canonical equations of orthosilicic acid speciation in water (Iler, 1979; Rimstidt and Barnes, 1980; Sjöberg et al., 1981), or

$$H_4SiO_4 \leftrightarrow H_3SiO4^- + H^+ \qquad pK_{a1} = 9.472 \text{ (in 0.6 M NaCl)} \qquad (1)$$

$$H_3SiO_4^- \leftrightarrow H_2SiO4^{2-} + H^+ \qquad pK_{a2} = 12.650 \text{ (in 0.6 M NaCl)} \qquad (2)$$

do not give the complete picture. In particular, some molecules that have appeared in simulations and were considered reaction intermediates often are more energetically stable than the autoionization products given by equations (1) and (2). Also, these reaction intermediates are

intriguing compounds in themselves from the standpoint of biochemical reactions, as well as industry.

The present work aims to accomplish three things. First, a zwitterion form of orthosilicic acid is examined in the neutral pH regime. This zwitterion is derived from similar reaction intermediates reported ~~at~~ by Mondal et al. (2009) and Zhou et al. (2002) . Second, its relevance in the dimerization reaction of silica through representative reactions is investigated. Third, the effects of explicitly adding sodium chloride to the system are evaluated. It is therefore envisaged that the dimerization proceeds as depicted in Figure 1.

2.0 Methodology and Theory

Density functional theoretical calculations were performed on constructed model systems using the Gaussian 16 suite of programs (Frisch et al., 2016) running in Dell PowerEdge M620 servers. The three-parameter hybrid functional B3LYP method was utilized and two types of basis sets were used: one which purely uses 6-311++G(d,p) on all atoms, and another which is a customized combination of 6-311++G(d,p) and 6-31+G(d) on specified atom centers, henceforth designated 6-311++G(d,p)[36]/6-31+G(d), where "[36]" represents the number of atom centers to which 6-311++G(d,p) are applied. The use of the B3LYP method and the 6-311++G(d,p) basis set together is mainly because they are known to produce good estimates of thermochemistry for silicate systems (Cypryk and Gostynski, 2016) and because their use would facilitate the ease of comparison with previous studies (e.g., Cheng et al., 2012; Criscenti et al., 2006; Alkorta et al.,

2001). The use of 6-311++G(d,p)[36]/6-31+G(d) was used for the bigger chemical systems for computing tractability, and is similar to the method that was evaluated by Yang et al. (2009).

The initial model systems, or configurations of atoms, were prepared as follows:

1. The starting configuration of the "pure-water" model simulation was constructed first. Twenty-seven water molecules were added randomly and evenly around an H_4SiO_4 molecule. The resulting system was optimized at 6-31+G(d) and subsequently to the desired level of 6-311++G(d,p).

2. Another H_4SiO_4 was added to the system above and thirty-one water molecules were added randomly and evenly around. The resulting system was optimized at 6-31+G(d) and subsequently to the desired level of 6-311++G(d,p)[36]/6-31+G(d). The choice of the thirty-six atoms that made use of the higher 6-311++G(d,p) basis sets was done from defining a reaction center – the set of molecules with the anticipated bond-breaking and bond formation and the immediately neighboring water molecules. This is the starting configuration of the pure-water model for dimerization.

3. Atoms of Na and Cl were added to the two systems above, leading to two additional systems. The placements of the two atoms were arbitrary but juxtaposed to each other. These systems were likewise optimized to the respective desired basis sets.

The four resulting systems from the procedure described above were clusters of molecules that had 90, 92, 195 and 197 atoms each. Constrained optimizations were performed on the structures to determine other minima and first order saddle-points in between them. Transition state optimizations were done with the synchronous transit-guided quasi-Newton method at the

respective basis sets mentioned above, followed by vibrational frequency calculations to establish that structures are true saddle points. All minima were fully optimized and analyzed for harmonic vibrational frequencies and zero-point energies. Optimization calculations yield stationary points that are internal energy minima along a potential energy surface (PES), which is a hypothetical surface where vibrations are absent. However, even in the ground state, a chemical system would have a ground state energy or zero-point energy. Hence, internal energies need to be corrected and form another surface that is elevated in energy from the PES, or a zero-point energy corrected PES. While the two surfaces might have similar topologies, this may not always be the case particularly in the case of shallow potential energy wells.

Free energies were evaluated by frequency calculations at 298.15K and 1 atm. Note that the equilibrium constant K, and pK are related to the ΔG of the net overall reactions by

$$K = - \exp(-\Delta G/\mathrm{R}T) \text{ and} \quad (3)$$

$$\mathrm{p}K = - \log (K) \quad (4)$$

Atomic charge distributions were accomplished by Hirshfeld population analysis (Hirshfeld, 1977), and CM5 calculations (Marenich et al. 2012; Wiberg and Rablen, 2018). The more common Mulliken (1955) population analyses results were not reported as it is considered sensitive to basis set size and to the choice of basis (Marenich et al. 2012) and deemed less reliable than either Hirshfeld or CM5.

3.0 Results

The computations in this study resulted in a total of eighteen fully optimized energy minima and thirteen associated intervening fully optimized first-order saddle points that connect the paths of the reactions of interest; these are all referred to as "stationary points". The fully optimized minima represent reactants, products, and intermediates, and the first-order saddle points represent transition states. These stationary points are in four distinct systems each with their own elemental compositions and assigned basis sets. Relative energy changes were calculated between stationary points along a reaction path within each system only. The complete set of configurations are listed in the supplement. Note that these discovered pathways are a sampling of possible mechanisms and are not an exhaustive list. However, they determine the current best upper bounds to activation energies because competing pathways would need to have reaction rates that are equal to or greater than these mechanisms.

3.1 Pure water: $H_4SiO_4 + 27H_2O$ system

There were two species of silica that can be identified in this system through following reaction paths and exploring the PES. As expected from numerous previous DFT and ab initio studies, orthosilicic acid is one of these species. The other species is a zwitterion isomer of orthosilicic acid, which henceforth will be referred to as orthosilicic acid zwitterion ($SiO^-(OH)_2(H_2O)^+$, or OSAZ). Initial configurations having $H_3SiO_4^-$ and free H^+ did not stabilize but optimized to either OSAZ or H_4SiO_4.

There are twelve possible tetrahedral arrangements for two –OH groups, one $–O^-$ group and one $–OH_2^+$- group around a silicon atom. For computational practicality therefore, only one of these combinations was arbitrarily chosen for determining the isomer transformation path. An energetically viable path for the transformation between the two minima was determined and is

shown in Figure 2; the corresponding change in energies for the elementary and net reactions are listed in Table 1.

	ΔU	ΔU_{zpc}	ΔG_{298}	pK_{298}
A. H_4SiO_4 + 27H_2O system				
Elementary reactions:				
(1) H_4SiO_4 (A) → [AB]‡	14.14	11.10	13.58	
(2) $SiO^-(OH)_2(H_2O)^+$ (B) → [AB]‡	3.867	2.004	2.981	
Net reaction:				
H_4SiO_4 ↔ $SiO^-(OH)_2(H_2O)^+$	10.27	9.092	10.60	7.776
B. H_4SiO_4 + 27H_2O + NaCl system				
Elementary reactions:				
(1) H_4SiO_4 (C) → [CD]‡	7.476	5.600	9.997	
(2) H_3O^+•H_2O•$H_3SiO_4^-$ (D) → [CD]‡	1.347	-1.088	0.869	
(3) H_3O^+•H_2O•$H_3SiO_4^-$ (D') → [DD']‡	9.394	5.845	4.933	
Net reaction:				
H_4SiO_4 ↔ H_3O^+•H_2O•$H_3SiO_4^-$	6.129	6.688	9.128	6.694

Table 1. Energies for elementary reactions and net reaction. Units are kcal/mol. All are computed in the B3LYP/6-311++G(d,p) level. The dot (•) signifies hydrogen bonding. Elementary reaction energy changes are pseudo-thermodynamic and are denoted by a double-dagger superscript ‡ (e.g. $\Delta U^{‡}$).

Presented are the internal energy changes (ΔU), the internal energy changes corrected for zero-point energies (ΔU_{zpc}) and the Gibbs free energy changes at 298K (ΔG_{298}). The pK is also evaluated at 298K from equations (3) and (4).

The computed net free energy indicates that the forward reaction from orthosilicic acid to OSAZ is less favored than the reverse reaction. The forward reaction has a relatively higher activation energy barrier than the reverse reaction and, consequently, the transition state is configurationally more similar with OSAZ.

No stationary points that represent free protons (H^+), hydronium ion (H_3O^+) or dihydroxonium ions ($H_5O_2^+$) were found in this pure water system even with optimization runs with initial configurations with them present. While this does not demonstrate non-existence of these local

minima, it suggests that if these positively charged aqueous species ever do exist, they may be occurring in very shallow PES wells where configurations can easily evolve to more favored species. It also suggests that the pure water case is less conducive to their formation.

3.2 Salt present: $H_4SiO_4 + 27H_2O + NaCl$ system

There were two species of silica that can be identified in this system through following reaction paths and exploring the PES. Aside from orthosilicic acid, configurations of $H_3SiO_4^-$, which are charge balanced by a hydronium ion (H_3O^+) with a water molecule in between. For clarity, this is denoted as $H_3O^+ \bullet H_2O \bullet H_3SiO_4^-$, where the dot • refers to hydrogen bonding. The hydrogen bonds are 1.4A to 1.7A in length. Attempts to optimize OSAZ to a stationary point were not successful in this system.

The reaction path from orthosilicic acid to $H_3O^+ \bullet H_2O \bullet H_3SiO_4^-$ was computed. Because there are several possible configurations of $H_3O^+ \bullet H_2O \bullet H_3SiO_4^-$, a transformation path from one $H_3O^+ \bullet H_2O \bullet H_3SiO_4^-$ to another was also computed. The results are shown in Figure 3 and the corresponding energies are listed in Table 1.

To estimate the concentration of NaCl in the system being modeled, gross volume calculations were performed by defining the surface as the contour of 0.001 electrons/Bohr3 density and using a Monte Carlo integration method (Parsons and Ninham, 2009). This method yielded volumes of 490 cc/mole and 460 cc/mole for Figure 3.C and D respectively, corresponding to concentrations of 2.0M and 2.2M of NaCl. In comparison, saturated brine is 6.14M NaCl and seawater is 0.469 moles/kg NaCl (Culkin and Cox, 1966)

3.3 Dimerization in pure water: $2H_4SiO_4 + 60H_2O$ system

Four species of silica were identified in this system through following the reaction paths and exploring the PES. Namely, these species are orthosilicic acid, OSAZ, $H_3SiO_4^-$, and $H_6Si_2O_7$. Hence, there are potentially at least six reaction paths that can be explored in this system. The focus however is to find the relevance of OSAZ to the dimerization reaction and to the other three species, and therefore not all reaction paths were investigated. The calculated paths are shown in Table 2.

	$\Delta U^{\ddagger}$	$\Delta U^{\ddagger}_{zpc}$	$\Delta G^{\ddagger}_{298}$	
A. $2H_4SiO_4 + 60H_2O$				
Elementary reactions:				
(1) $2H_4SiO_4$ (A) $\rightarrow$ [AB]‡	21.65	16.89	17.46	
(2) $SiO^-(OH)_2(H_2O)^+ + H_4SiO_4$ (B) $\rightarrow$ [AB]‡	5.475	1.744	1.899	
(3) $SiO^-(OH)_2(H_2O)^+ + H_4SiO_4$ (B) $\rightarrow$ [BC]‡	4.561	4.474	5.849	
(4) $SiO^-(OH)_2(H_2O)^+ \bullet H_4SiO_4$ (C) $\rightarrow$ [BC]‡	1.413	2.684	3.972	
(5) $SiO^-(OH)_2(H_2O)^+ \bullet H_4SiO_4$ (C) $\rightarrow$ [CD]‡	9.643	10.66	11.85	
(6) $H_6Si_2O_7$ (D) $\rightarrow$ [CD]‡	31.24	30.14	32.14	
(7) $SiO^-(OH)_2(H_2O)^+ \bullet H_4SiO_4$ (C) $\rightarrow$ [CE]‡	0.194	-0.597	0.188	
	0.085	-0.644	0.105	*
(8) $H_3O^+ \bullet H_3SiO_4^- \bullet H_4SiO_4$ (E) $\rightarrow$ [CE]‡	0.078	-0.937	-0.553	
	0.209	-1.006	-0.754	*
(9) $H_3O^+ \bullet H_3SiO_4^- \bullet H_4SiO_4$ (E) $\rightarrow$ [EF]‡	7.090	5.228	5.939	
	6.821	4.618	5.189	*
(10) $H_3O^+ + H_3SiO_4^- \bullet H_4SiO_4$ (F) $\rightarrow$ [EF]‡	0.193	-1.369	-0.911	
	0.336	-1.537	-1.062	*
B. $2H_4SiO_4 + 60H_2O + NaCl$				
Elementary reactions:				
(1) $2H_4SiO_4$ (G) $\rightarrow$ [GH]‡	18.21	14.28	15.24	
(2) $SiO^-(OH)_2(H_2O)^+ + H_4SiO_4$ (H) $\rightarrow$ [GH]‡	5.451	2.866	3.328	
(3) $SiO^-(OH)_2(H_2O)^+ + H_4SiO_4$ (H) $\rightarrow$ [HI]‡	10.11	11.98	14.63	
(4) $H_6Si_2O_7$ (I) $\rightarrow$ [HI]‡	25.65	26.53	29.61	
(5) $SiO^-(OH)_2(H_2O)^+ + 2H_2O$ (H) $\rightarrow$ [HJ]‡	7.816	6.520	8.152	
(6) $H_3O^+ + H_3SiO_4^-$ (J) $\rightarrow$ [HJ]‡	6.876	4.592	4.962	

Table 2. Energies for elementary reactions. Units are kcal/mol. All are computed with the B3LYP method and a custom basis set from a combination of 6-311++G(d,p) and 6-31+G(d) basis sets. The dot (•) signifies hydrogen bonding. The asterisk '*' indicates recalculation in a new basis set with a reassignment of atom centers.

Table 2.A and Figure 4 show one possible mechanism to dimerization under neutral pH in pure water. The process begins with two H_4SiO_4 molecules sitting side-by-side. Next, one of the

H_4SiO_4 molecules transforms to OSAZ. Subsequently, H-bonding draws the two different silica molecules closer together. Finally, the H_4SiO_4 molecule simultaneously donates a proton, performs a nucleophilic attack on the silicon of OSAZ, and causes the H_2O group of OSAZ to eject.

Figure 5 shows the formation of $H_3SiO_4^-$ from OSAZ. Note that the $H_3SiO_4^-$ species is charge balanced by the immediately neighboring H_3O^+ formed from the freed proton (Figure 5.E). A second configuration where H_3O^+ is more distant (Figure 5.F) was also found. The energy profiles corresponding to the configurations in Figures 4 and 5 are shown in Figure 6.

Because the bond breaking and bond formation during $H_3SiO_4^-$ production (Figure 6 C-E-F) involve atoms that were not among the thirty-six that were initially assigned the high basis set, a reassignment of basis sets on atom centers was done and subsequent optimization and frequency calculations were performed to test the reliability of the results. This procedure led to a second (though generally similar) energy curve (Table 2.A.7-10) and to almost identical configuration geometries, based on RMSD of 0.020A-0.028A; here, the RMSD was determined by Kabsch algorithm (Kabsch, 1976). The elementary reaction in Table 2.A.9 was the most sensitive to this reassignment and change in basis, exhibiting a free energy difference of only 0.75 kcal/mol.

	ΔU	ΔU_{zpc}	ΔG_{298}	pK_{298}
A. $2H_4SiO_4 + 60H_2O$				
Net reactions:				
(1) $2H_4SiO_4$ (A) $\leftrightarrow H_6Si_2O_7 + H_2O$ (D)	-2.279	-2.546	-2.847	-2.088
(2) $2H_4SiO_4$ (A) $\leftrightarrow SiO^-(OH)_2(H_2O)^+ + H_4SiO_4$ (B)	16.17	15.14	15.56	11.41
(3) $2H_4SiO_4$ (A) $\leftrightarrow SiO^-(OH)_2(H_2O)^+ \bullet H_4SiO_4$ (C)	19.32	16.93	17.44	12.79
(4) $2H_4SiO_4$ (A) $\leftrightarrow H_3O^+ \bullet H_3SiO_4^- \bullet H_4SiO_4$ (E)	18.53	16.50	17.51	12.84
(5) $2H_4SiO_4$ (A) $\leftrightarrow H_3O^+ + H_3SiO_4^- \bullet H_4SiO_4$ (F)	25.43	23.10	24.36	17.86
B. $2H_4SiO_4 + 60H_2O + NaCl$				
Net reaction:				
(1) $2H_4SiO_4$ (G) $\leftrightarrow H_6Si_2O_7 + H_2O$ (I)	-2.779	-3.135	-3.070	-2.251

(2) $2H_4SiO_4$ (G) ↔ $SiO^-(OH)_2(H_2O)^+ + H_4SiO_4$ (H)	12.76	11.41	11.91	8.734
(3) $2H_4SiO_4$ (G) ↔ $H_3O^+ + H_3SiO_4^-$ (J)	13.70	13.34	15.10	11.07

Table 3. Energies for net reactions. Units are kcal/mol. All are computed with the B3LYP method and a custom basis set from a combination of 6-311++G(d,p) and 6-31+G(d) basis sets. The dot (•) signifies hydrogen bonding.

Net reactions and thermodynamic quantities are shown in Table 3. The dimerization reaction (Table 3.A.1) is thermodynamically favored. OSAZ that is hydrogen bonded to H_4SiO_4 is less favored.

3.4 Dimerization with salt present: $2H_4SiO_4 + 60H_2O$ + NaCl system

As with the dimerization in pure water system, four species of silica were identified in this system through following the reaction paths and exploring the PES: orthosilicic acid, OSAZ, $H_3SiO_4^-$, and $H_6Si_2O_7$. Similar to section 3.3, only the dimerization reaction of OSAZ is pursued because it the primary interest in this study. The calculated paths are shown in Table 2.

Table 2.B and Figure 7 show one possible mechanism to dimerization in neutral pH with NaCl present. The process begins with two H_4SiO_4 molecules sitting side-by-side. Next, one of the H_4SiO_4 molecules transforms to OSAZ. Finally, the H_4SiO_4 molecule simultaneously performs a nucleophilic attack on the silicon of OSAZ, transfers a proton via concerted reaction to the OSAZ oxygen, and causes the H_2O group of OSAZ to eject.

Figure 8 shows the formation of $H_3SiO_4^-$ from OSAZ. Note that the $H_3SiO_4^-$ species is charge balanced by a distant H_3O^+ formed by concerted transfers from the freed proton (Figure 8.J). The energy profiles corresponding to the configurations in Figures 7 and 8 are shown in Figure 9.

318 Although the production of $H_3SiO_4^-$ involved bond breaking and formation between atom centers
319 that were not initially assigned the higher basis set, and unlike what was done in section 3.3, test
320 on the reassignment of atom centers to the higher basis set was not performed. This was decided
321 because the reassignment procedure in the previous pure water case did not significantly modify
322 the reaction direction or the optimized geometries and, therefore, it is surmised that altering the
323 atom centers of the basis sets would not change the general findings regarding OSAZ reactivity.

324 Estimating concentrations by computing the molar volumes using the method of Parsons and
325 Ninham (2009) yielded volumes of 1033 cc/mole and 1069 cc/mole for Figure 7.G and I
326 respectively, corresponding to NaCl concentrations of 0.967M and 0.935M of NaCl. Likewise,
327 H_4SiO_4 concentrations are double these numbers at 1.934M and 1.870M and are 3 orders of
328 magnitude higher than saturation ($1.25x10^{-3}$M; Alexander et al., 1954).

329

330 4.0 Discussion

331 4.1 OSAZ

332 Configurationally, OSAZ is what would result if one of the hydrogen atoms from a hydroxide
333 group was moved to another hydroxide in orthosilicic acid resulting in a molecule with an $–O^-$
334 group and a $–H_2O^+$ group. This is essentially the reaction in Figure 2, where the movement of
335 proton occurs through concerted transfers facilitated by surrounding water molecules.

336 An examination of Lewis formal charges of OSAZ (Figure 2) yields a positive charge on the
337 $–OH_2$ group and a negative charge on the –O group. This doubly charged molecule is the

zwitterion state. To confirm the zwitterion characteristics of OSAZ, Hirshfeld and CM5 calculations were conducted on the configurations exhibited in Figure 2.A and Figure 2.B. The results are shown in Table 4. Upon transformation to OSAZ, the $-OH_2$ group assumes a positive charge and the -O group takes on a relatively high negative charge.

	Orthosilicic Acid:			Orthosilicic Acid Zwitterion:		
Center	Group	Hirshfeld	CM5	Group	Hirshfeld	CM5
Si	=Si=	0.5414	0.4921	=Si=	0.5095	0.4629
O	-OH	-0.1595	-0.1443	$-O^-$	-0.3679	-0.4599
O	-OH	-0.1505	-0.1479	$-OH_2^+$	0.05479	0.1868
O	-OH	-0.1457	-0.1377	-OH	-0.1488	-0.1431
O	-OH	-0.1475	-0.1421	-OH	-0.1423	-0.1405

Table 4 Charges on atom centers of orthosilicic acid and OSAZ in the pure water system from Hirshfeld population analysis and charge model 5. (Hirshfeld, 1977; Wiberg and Rablen, 2018) Hydrogen charges are summed into the oxygen atoms. Units are in atomic units.

Note that the magnitude of the charges differs between the Hirshfeld and CM5 results for the $-OH_2$ group. The CM5 method is considered a more reliable estimate than the Hirshfeld method (Marenich et al., 2012) and what is crucial is the direction of change. The sums of the charges are non-zero and slightly negative, whereas the molecule is expected to be neutral. This is likely due to a numerical artifact because the electron density distribution disperses the charges throughout the 90-atom system.

While the recognition of the zwitterion characteristics of OSAZ is new, similar structures have been seen in previous work (Zhou et al., 2002; Mondal et al., 2009). Table 5 compares Si-O bond lengths of these similar structures.

H_2O–Si	Si-OH	Reference
1.978	1.653	Zhou et al. (2002)
1.986	1.633-1.651	Mondal et al. (2009)

1.715/1.758	1.653-1.666	This study	

Table 5. Bond lengths of OSAZ compared to similar structures in previous studies. Units are in angstroms.

Orthosilicic acid and OSAZ differ in their intramolecular Si-O bond lengths and O-Si-O bond angles. In general, orthosilicic acid has tetrahedral symmetry having ∠O-Si-O of 109.5º and uniform Si-O bond lengths of 1.630A-1.663A. For OSAZ, the ∠O-Si-O angles are 105.8º for HO-Si-OH, 103.4º on average for H_2O^+-Si-OH, and 111.8º for H_2O^+-Si-O^-; the bond lengths vary significantly from 1.587A for Si-O^-, 1.653A-1.666A for Si-OH, and 1.715A for Si-OH_2^+.

OSAZ has a superficial resemblance to mono-hydrated metasilicic acid H_2O•($SiO(OH)_2$) although its geometry is distinct. In OSAZ, four oxygens are covalently bonded around a silicon atom in a distorted tetrahedron, whereas in metasilicic acid, three covalently bonded oxygen atoms are trigonal planar with silicon (Chelikowsky, 1998). Interestingly, metasilicic acid is observed in gas phase ab initio studies, whereas OSAZ-like structures are observed when water molecules are explicitly added to simulations (e.g., Mondal et al., 2009; Zhou et al. 2002). Ab initio studies of gas phase metasilicic acid (Mondal et al., 2009) show a H_2O-Si bond that is significantly longer (~1.9A) compared to OSAZ (~1.7A) for OSAZ. These seem to suggest that relaxation of the structure to a more tetrahedral geometry from a trigonal planar one is facilitated by the hydrogen bonds provided by water molecules surrounding the molecule. Furthermore, metasilicic acid is not known to experimentally exist in the aqueous phase, although it has been identified in steam (Hildenbrand and Lau, 1994).

4.2 Discussion on H_4SiO_4 + $27H_2O$ +/- NaCl systems: zwitterion formation

The models in these systems, where a lone H_4SiO_4 interacts with its aqueous environment, are intended to represent silica in dilute concentrations. The results of the calculations suggest that the zwitterion is more likely to be observed as a stable species where salts are in low concentration, while the auto-ionized $H_3SiO_4^-$ and H_3O^+ pair are more likely to be observed in elevated salt concentrations. This can be interpreted to mean that the polarizing effect of NaCl perturbs the stability of OSAZ and stabilizes the auto-ionization products.

The results suggests that one of the auto-ionized H_4SiO_4 structures in 2M NaCl is a dipolar complex, $H_3O^+ \bullet H_2O \bullet H_3SiO_4^-$ (Figure 3.D). The configuration, where the hydronium ion sits one water molecule away from the $H_3SiO_4^-$, is consistently reproducible (e.g., Figure 3.D') in this system. The existence of H_3O^+ is corroborated by theoretical (Meraj and Chaudhari, 2014) and empirical studies (Amir et al., 2007; Artemov et al., 2020).

Note that the pK_a of 6.694 for net reaction in Table 1.B is much lower than values reported by Sjöberg et al. (1981; pK_{a1}=9.472, Equation 1) and similarly values derived from the equations of Fleming and Crerar (1982; pK_{a1}=9.687). However, the pK_a value is in close agreement to that derived from amorphous silica titration experiments by von Schindler and Kamber (1968; pK_{a1}=6.8) and near the calculated values of –OH groups on the surface of quartz (Sulpizi et al., 2012; pK_a=5.5). These relationships need further investigation especially since different sites in silica appear to have different acidities. It may well be that the dipolar complex is another species whose concentration is three orders more than the fully ionized $H_3SiO_4^-$. It is interesting to note that the pK of the formation of the zwitterion (pK=7.776) is within these ranges and that therefore the concentration of zwitterion is only about one order of magnitude less than the dipolar complex.

411 The kinetics can be evaluated using transition state theory from the Gibbs free energy of
412 activation, which is related to the rate constant by

413 $$k = k_B T/h \exp(-\Delta G^{\ddagger}/RT) \quad (5)$$

414 where k_B is Boltzmann's constant, R is the gas constant, T is the temperature and h is Planck's
415 constant. The rate constants indicate that at the neutral pH regime, dilute silicate concentrations
416 and low salt concentrations, OSAZ is present as an isomer of H_4SiO_4 because equilibration
417 achieves completion in most surface conditions. The rate constant corresponding to the forward
418 reaction in Table 1.A.1with a free energy of 13.58 kcal/mol at 298K is 677 s^{-1}, indicating an
419 equilibration time of 1.48 milliseconds. The reverse reaction in Table 1.A.2 with a free energy of
420 2.981 is 4.04×10^{10} s^{-1} or 2.47×10^{-11} s. Rate constant calculations for the auto-ionization reactions
421 Table 1.B.1 and Table 1.B.2 are of similar magnitudes and therefore reaction completion times
422 are also rapid.

423 4.3 Discussion of $2H_4SiO_4 + 60H_2O$ (+/-) NaCl systems: dimerization by zwitterion

424 The models in these systems, where two H_4SiO_4 molecules are mutually interacting in an
425 aqueous environment, are intended to explore the dimerization reaction, and therefore to
426 investigate situations where the local concentration of silica is sufficient to enable encounters
427 between H_4SiO_4 molecules. This can be at super-saturation, at the water-mineral interface, or
428 chance encounters due to diffusion. The results of the calculations show that in the presence of a
429 neighboring H_4SiO_4, OSAZ and the auto-ionized products, $H_3SiO_4^-$ and H_3O^+, simultaneously
430 occur with or without the presence of NaCl. This is in contrast with the results of the "dilute"
431 system from the previous section (4.2) where the occurrence of OSAZ is exclusive of the

occurrence of $H_3SiO_4^-$ and H_3O^+, and vice versa, which admittedly may be an artifact of the system size of the simulation. Another difference is that in the dilute system, auto-ionization is favored over zwitterion formation, whereas the reverse is true here.

The free energy differences between the two monomers and the dimer in both the pure water system and the system with NaCl (reactions Table 3.A.1 and 3.B.1) indicate that the dimer is slightly thermodynamically more favored, corresponding to a pK_{298} of -2.088 and -2.25, respectively. The direction of reaction favorability is similar to Noguera et al. (2015) who computed pK_{303}=-0.69. Some workers (Exley and Sjöberg, 2014; Sjöberg et al., 1981) however expressed that the monomer should be slightly more preferred. This deserves further exploration in the future.

Note that in the pure water case, the occurence of OSAZ is thermodynamically slightly more preferred over $H_3SiO_4^-$ (Table 3.A.3 and 3.A.4) and this preference is enhanced when NaCl is present (Table 3.B.2 and 3.B.3). These observations are crucial since temporal concentrations factor into the rate and OSAZ is being evaluated as a competitor to the other silica species for the dimerization reaction.

The dimerization mechanism involving zwitterion proceeds differently from previous mechanisms proposed. Instead of forming a chemically reactive nucleophile, the conversion to the zwitterion isomer turns the monomer into a target for nucleophilic attack by a neighboring H_4SiO_4. This type of mechanism can be more easily extended to oligomerization as all it needs is a dangling –OH group from the other reactant.

The rate determining step for the neutral pH dimerization process has a zero-point corrected activation energy of 16.89 kcal/mol for the pure water system and 14.28 kcal/mol for the NaCl present system, which strongly suggests that the zwitterion pathway is a good candidate for the dimerization mechanism in neutral pH. According to experimental studies (Rothbaum and Rohde, 1979; Makrides et al., 1980), the activation energy for this reaction should be between 3 kcal/mol and 17 kcal/mol and therefore, the results of this study are in excellent agreement with experiment. In comparison, the mechanism by reported by Trinh et al. (2006) has an activation energy of 30.4 kcal/mol for the rate-determining step, while that of Liu et al. (2019) has an activation energy of 31.8 kcal/mol.

Comparison with the experimental values of the reverse mechanism, or hydrolysis, is also interesting. The activation energies of the rate-determining step in this study are 30.14 kcal/mol for the pure water system and 26.53 kcal/mol for the NaCl present system, and are slightly lower compared to other studies. Trinh et al Trinh 32.74 kcal/mol. and Xiao and Lasaga (1994) has an activation energy of 28.51 kcal/mol for the neutral reaction. According to experimental studies (Walther, 1996; Knauss and Wollery, 1988; Brady and Walther, 1990; Dove and Crerar, 1990), the activation energy for the hydrolysis reaction should be between 16 and 22 kcal/mol and therefore the pertinent activation energies in this study (reactions in Table 2.A.6 and Table 2.B.4) are still too high. However, remember that the rate-determining step, which controls the overall rate, is the step with the highest activation energy, and therefore the overall rate can be made faster by breaking up a high activation energy step into smaller lower activation energy steps. It is therefore for future work to show that the involvement of water molecules breaks up the D-$[CD]^{\ddagger}$ (pure water) step and the I-$[HI]^{\ddagger}$ (NaCl present) step into smaller steps.

One intriguing aspect of the simulation is that, although all the points were optimized to local minima and transition states, and while all paths to transition states from their respective local minima yield positive changes in internal energy changes ($\Delta U^{\ddagger}$), the zero-point corrected activation energies ($\Delta U^{\ddagger}_{zpc}$) in the equations in Table 2.A.7, 8 and 10 yield negative values and the Gibbs free energy of activation ($\Delta G^{\ddagger}_{298}$) for equation in Table 2.A.8 and 10 are also negative. These are likely due to the shallowness of the potential energy wells of the configurations of H_3O^+; it may also be a consequence of the mobility of the proton. However, the true PES is a surface of zero-point corrected points. Therefore, the energy optimized nature of the stationary points in Figure 4.E, F, $[CE]^{\ddagger}$ and $[EF]^{\ddagger}$ need to be approached with caution.

5.0 Conclusion

The speciation of silica in surface waters is almost universally acknowledged to be predominantly defined by equations (1) and (2), and hence, the recognized main species of monomeric silica are H_4SiO_4, H_3SiO4^- and H_2SiO4^{2-}. The results of this study suggest that there is at least a third reaction that needs to be considered,

$$H_4SiO_4 \leftrightarrow SiO^-(OH)_2(H_2O)^+ \qquad pK=7.7 \qquad (6)$$

and therefore there is a fourth monomeric silica species, $SiO^-(OH)_2(H_2O)^+$ or OSAZ, that is present in solution in appreciable amounts relative to the previous three. Furthermore, this fourth species is a likely participant in the dimerization process.

6.0 Acknowledgments

All computations in this study were performed on Yale high-performance computing servers and the author wishes to thank Mark Gerstein and Yale University for the use of these. The author thanks Prashant Emani and Declan Clarke for proofreading the text and giving invaluable comments. This research did not receive any specific grant from funding agencies in the public, commercial, or not-for-profit sectors.

7.0 References

Alexander G. B., Heston W. M. and Iler H. K. (1954) The solubility of amorphous silica in water. *J. Phys. Chem.*, **58**, 6, 453–455.

Alkorta I., Rozas I. and Elguero J. (2001) Molecular Complexes between Silicon Derivatives and Electron-Rich Groups. *J. Phys. Chem. A*, **105**, 4, 743–749.

Amir W., Gallot G., Hache F., Bratos S., Leicknam J. and Vuilleumier R. (2007) Time-resolved observation of the Eigen cation in liquid water. *J. Chem. Phys.,* **126**, 034511.

Artemov V. G., Uykur E., Roh S., Pronin A. V., Ouerdane H. and Dressel M. (2020) Revealing excess protons in the infrared spectrum of liquid water. *Sci. Rep.*, **10**, 11320-11329.

Brady P. V. and Walther J. V. (1990) Kinetics of quartz dissolution at low temperatures. *Chem. Geol*., **82**, 253-264.

Burkett S. L. and Davis, M. E. (1995) Mechanisms of Structure Direction in the Synthesis of Pure-Silica Zeolites. 1. Synthesis of TPA/Si-ZSM-5. *Chem. Mater.*, **7**, 1453–1463.

Car R. and Parinello M. (1985) Unified Approach for Molecular Dynamics and Density-Functional Theory. *Phys. Rev. Lett.*, **55,** 2471–2474.

Chelikowsky J. R. (1998) Structural and electronic properties of neutral and charged silicalike clusters. *Phys. Rev. B*, 57, 3333-3339.

Cheng X., Chen D. and Liu Y. (2012) Mechanisms of silicon alkoxide hydrolysis-oligomerization reactions: a DFT investigation. *Chemphyschem,* **13**, 9, 2392-2404.

Criscenti L. J., Kubicki, J. D. and Brantley S. L. (2006) Silicate glass and mineral dissolution: calculated reaction paths and activation energies for hydrolysis of a Q^3 Si by H_3O^+ using ab initio methods. *J. Phys. Chem. A*, **110**, 198-206.

Culkin F. and Cox R. A. (1966) Sodium, potassium, magnesium, calcium and strontium in sea water. *Deep-Sea Res.*, **13**, 789-804.

Cypryk M. and Gostynski B. (2016) Computational benchmark for calculation of silane and siloxane thermochemistry. *J. Mol. Model.,* **22**, 1, 35.

529 Dove P. M. and Crerar D. A. (1990) Kinetics of quartz dissolution in electrolyte-solutions using
530 a hydrothermal mixed flow reactor. *Geochim. Cosmochim. Acta,* **54**, 1267-1281.

531 Exley C, Sjöberg S. (2014) Silicon species in seawater. *Spectrochim. Acta A Mol Biomol*
532 *Spectrosc.* **117**, 820-821.

533 Felipe M. A., Kubicki J. D. and Rye D. M. (2004) Oxygen isotope exchange kinetics between
534 water and dissolved silica from ab initio calculations. *Geochim. Cosmochim. Acta*, **68**, 949-
535 958.

536 Fleming B. A. and Crerar D. A. (1982) Silicic acid ionization and calculation of silica solubility
537 at elevated temperature and pH application to geothermal fluid processing and reinjection.
538 *Geotherm.,* **II**, l, 15-29.

539 Frisch M. J., Trucks G. W., Schlegel H. B., Scuseria G. E., Robb M. A., Cheeseman J. R.,
540 Scalmani G., Barone V., Petersson G. A., Nakatsuji H., Li X., Caricato M., Marenich A. V.,
541 Bloino J., Janesko B.G., Gomperts R., Mennucci B., Hratchian H. P., Ortiz J. V., Izmaylov
542 A. F., Sonnenberg J. L., Williams-Young D., Ding F., Lipparini F., Egidi F., Goings J., Peng
543 B., Petrone A., Henderson T., Ranasinghe D., Zakrzewski V. G., Gao J., Rega N., Zheng G.,
544 Liang W., Hada M., Ehara M., Toyota K., Fukuda R., Hasegawa J., Ishida M., Nakajima T.,
545 Honda Y., Kitao O., Nakai H., Vreven T., Throssell K., Montgomery J. A. Jr., Peralta J. E.,
546 Ogliaro F., Bearpark M. J., Heyd J. J., Brothers E. N., Kudin K. N., Staroverov V. N., Keith
547 T. A., Kobayashi R., Normand J., Raghavachari K., Rendell A. P., Burant J. C., Iyengar S. S.,
548 Tomasi J., Cossi M., Millam J. M., Klene M., Adamo C., Cammi R., Ochterski J. W., Martin
549 R. L., Morokuma K., Farkas O., Foresman J. B., and Fox D.J. (2019) *Gaussian 16, Revision*
550 *C.01*. Gaussian, Inc., Wallingford CT

551 Gorrepati E. A., Wongthahan P, Raha S. and Fogler H. S. (2010) Silica precipitation in acidic
552 solutions: Mechanism, pH effect, and salt effect. *Lang.*, **26**, 13, 10467-10474.

553 Goto K. (1956) Effect of pH on polymerization of silicic acid. *J. Phys. Chem*., **60**, 7, 1007-1008.

554 van Grotthuss C. J. T. (1806). Sur la décomposition de l'eau et des corps qu'elle tient en
555 dissolution à l'aide de l'électricité galvanique. *Ann. Chim.* **58**, 54–73.

556 Harrison C. C. and Loton N. (1995) Novel routes to designer silicas: studies of the
557 decomposition of $(M^+)_2[Si(C_6H_4O_2)_3]\cdot xH_2O$. Importance of M^+ identity of the kinetics of
558 oligomerisation and the structural characteristics of the silicas produced. *J. Chem. Soc.,*
559 *Faraday Trans*., **91**, 4287–4297.

560 Heenen H. H., Gauthier J. A., Kristoffersen H. H., Ludwig T. and Chan K. (2020) Solvation at
561 metal/water interfaces: An ab initio molecular dynamics benchmark of common
562 computational approaches. *J. Chem. Phys.,* **152**, 144703.

563 Hildenbrand D. L. and Lau K. H. (1994) Thermochemistry of gaseous $SiO(OH)$, $SiO(OH)_2$, and
564 SiO_2. J. Chem. Phys., **101**, 6076.

565 Hirshfeld F. L. (1977) Bonded-atom fragments for describing molecular charge densities. *Theor.*
566 *Chim. Acta*, **44**, 129–138.

567 Huˇs M. and Urbic T. J. (2012) Strength of hydrogen bonds of water depends on local
568 environment. *J. Chem. Phys.* **136**, 14, 144305.

Hu H., Hou H., He Z. and Wang B. (2013) Theoretical characterizations of the mechanism for the dimerization of monosilicic acid in basic solution. *Phys. Chem. Chem. Phys.*, **15**, 15027-15032.

Icopini G. A., Brantley S. L. and Heaney P. J. (2005) Kinetics of silica oligomerization and nanocolloid formation as a function of pH and Ionic Strength at 25ºC. *Geochim. Cosmochim. Acta*, **69**, 293-303.

Iler R. K. (1979) *The Chemistry of Silica.* Wiley, New York.

Izotova E. D., Rudakova M. A. and Akberova N. I. (2020) The molecular dynamics of silica acids in aqueous solution: Qualitative and quantitative characteristics of oligomers. *Uchenye Zapiski Kazanskogo Universiteta. Seriya Fiziko-Matematicheskie Nauk*i, **162**, 1, 5–26.

Kabsch W. (1976) A solution for the best rotation to relate two sets of vectors. *Acta Crystallog.*, **A32**, 922-923.

Kirk S. R., Yin D., Persson M., Carlen J. and Jenkins S. (2011) Molecular dynamics simulations of the aggregation of nanocolloidal amorphous silica monomers and dimers. *Procedia Eng.*, **18**, 188-193.

Knauss K. and Wolery T. (1988) The dissolution kinetics of quartz as a function of pH and time at 70 ° C. *Geochem. Cosmochim. Acta*, **52**, 43-53.

Jorge M., Gomes J. R. B., Natália M., Cordeiro D. S. and Seaton N. A. (2009) Molecular dynamics simulation of the early stages of the synthesis of periodic mesoporous silica. *J Phys Chem B,* **113**, 3, 708-18.

Liu X., Liu C. and Meng C. (2019) Oligomerization of silicic acids in neutral aqueous solution: a first-principles investigation. *Int. J. Mol. Sci.* **20**, 12, 3037.

Makrides A. C., Turner M. and Slaughter J. (1980) Condensation of silica from supersaturated silicic acid solutions. *J. Coll. Interf. Sci*., **73**, 2, 345-367.

Malani A., Auerbach S. M. and Monson P. A. (2010) Probing the mechanism of silica polymerization at ambient temperatures using Monte Carlo Simulations. *J. Phys. Chem. Lett.* **1**, 21, 3219-3224.

Martin P., Gaitero J. J., Dolado J. S. and Manzano H. (2021) New kinetic Monte Carlo model to study the dissolution of quartz. *ACS Earth Space Chem.* **5**, 3, 516-524.

Mondal B., Ghosh D., and Das A. K., (2009) Thermochemistry for silicic acid formation reaction: Prediction of new reaction pathway. *Chem. Phys. Lett.*, **478**, 4, 115-119.

Mora-Fonz M. J., Catlow C. R. A. and Lewis D. W. (2007) *J. Phys. Chem. C*, **111**, 49, 18155-18158.

Mulliken R. S. (1955) Electronic population analysis on LCAO–MO molecular wave functions. I. *J. Chem. Phys.*, **23**, 1833–1840.

Noguera C., Fritz B. and Clément A. (2015) Precipitation mechanism of amorphous silica nanoparticles: A simulation approach. J. Coll. Interf. Sci., 448, 553-563.

Pavlova A., Trinh T. T., van Santen R. A. and Meijer E. J. (2013) Clarifying the role of sodium in the silica oligomerization reaction. *Phys. Chem. Chem. Phys.,* **15**, 4, 1123-1129.

Pelmenschikov A.G., Morosi G. and Gamba A. (1997) Adsorption of water and methanol on silica hydroxyls: Ab initio energy and frequency calculations. *J. Phys. Chem. A,* **101**, 1178-1187.

Rimstidt J. D. and Barnes H. L. (1980) The kinetics of silica-water reactions. *Geochim. Cosmochim. Acta* **44**, 1683-1699.

Rimstidt J. D. (2015) Rate equations for sodium catalyzed quartz dissolution. *Geochim. Cosmochim. Acta* **167**, 195–204.

Rothbaum H. P. and Rohde A. G. (1979) Kinetics of silica polymerization and deposition from dilute solutions between 5 and 180°C. *J. Coll. Interf. Sci.*, **71**, 3, 533-559.

von Schindler P. and Kamber H. R. (1968) Die acidität von silanolgruppen. *Helv. Chim. Acta*, **51**, 1781-1786.

Sjöberg S., Nordin A. and Ingri N. (1981) Equilibrium and structural studies of silicon(IV) and aluminium(III) in aqueous solution. II. Formation constants for the monosilicate ions $SiO(OH)_3^-$ and $SiO_2(OH)_{22}^-$. A precision study at 25°C in a simplified seawater medium. *Mar. Chem.*, **10**, 6, 521-532.

Sulpizi M., Gaigeot M. and Sprik M. (2012) The silica–water interface: how the silanols determine the surface acidity and modulate the water properties. *J. Chem. Theory Comput.,* **8**, 3, 1037–1047.

Tossel J. (2005) Theoretical study on the dimerization of $Si(OH)_4$ in aqueous solution and its dependence on temperature and dielectric constant. *Geochim. Cosmochim. Acta*, **69**, 2, 283–291.

Trinh T. T., Jansen A. P. J., van Santen R. A. and Jan Meijer E. (2009) The role of water in silicate oligomerization reaction. *Phys. Chem. Chem. Phys.* **11**, 25, 5092-5099.

Trinh T. T., Jansen A. P. J. and van Santen R. A. (2006) Mechanism of Oligomerization Reactions of Silica. *J. Phys. Chem. B*, **110**, 23099-23106.

Walther J. V. (1996) Relation between rates of aluminosilicate mineral dissolution, pH, temperature, and surface charge. *Am. J. Sci.*, **296**, 693-728.

Wiberg K. B. and Rablen P. R. (2018). Atomic Charges. *J. Org. Chem.,* **83**, 24, 15463-15469.

Xiao Y. T. and Lasaga A. C. (1996) Ab initio quantum mechanical studies of the kinetics and mechanisms of quartz dissolution: OH^- catalysis. *Geochim. Cosmochim. Acta* **60**, 2283-2295.

Xiao Y. T. and Lasaga A. C. (1994) Ab-initio quantum-mechanical studies of the kinetics and mechanisms of silicate dissolution - $H^+(H_3O^+)$ catalysis. *Geochim. Cosmochim. Acta* **58**, 5379-5400.

Yang Y., Weaver M. N. and Merz K. M. Jr. 2009 Assessment of the "6-31+G** + LANL2DZ" mixed basis set coupled with density functional theory methods and the effective core potential: prediction of heats of formation and ionization potentials for first-row-transition-metal complexes. *J. Phys. Chem. A*, **113**, 36, 9843–9851

Zhang J., Zhang H., Wu T., Wang Q. and van der Spoel D. (2017) Comparison of Implicit and Explicit Solvent Models for the Calculation of Solvation Free Energy in Organic Solvents. *J Chem Theory Comput.,* **13**, 3, 1034-1043.

Zhou M., Zhang L., Lu H., Shao L. and Chen M. (2002). Reaction of silicon dioxide with water: A matrix isolation infrared and density functional theoretical study. *J. Mol. Struct.* **605**, 249–254.

Zhang X., van Santen R. A. and Jansen A. P. J. (2012) Kinetic Monte Carlo modeling of silicate oligomerization and early gelation. *Phys. Chem. Chem. Phys.*, **14**, 34, 11969-11973.

655 Figure 1. Proposed dimerization reaction and the analogous generalized oligomerization reaction.

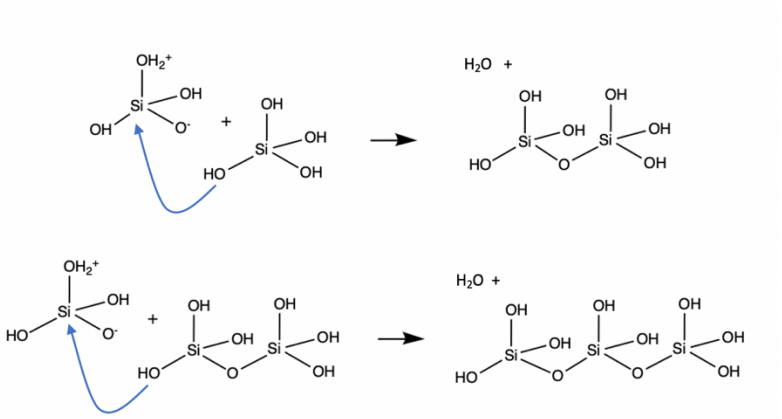

656

Figure 2. OSAZ formation. Pure water mechanism from orthosilicic acid (A) to OSAZ (B) optimized at the B3LYP/6-311++G(d,p) level. The corresponding energy changes are shown in Table 1.

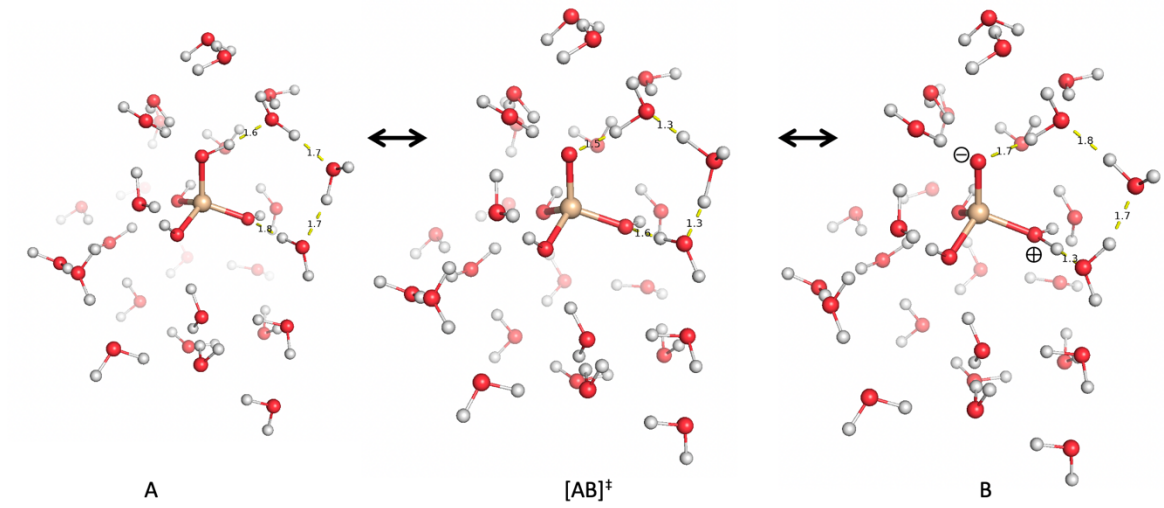

Figure 3. Auto-ionization. NaCl present mechanism from orthosilicic acid (C) to its auto-ionization products (D and D') optimized at the B3LYP/6-311++G(d,p) level. The corresponding energy changes are shown in Table 1.

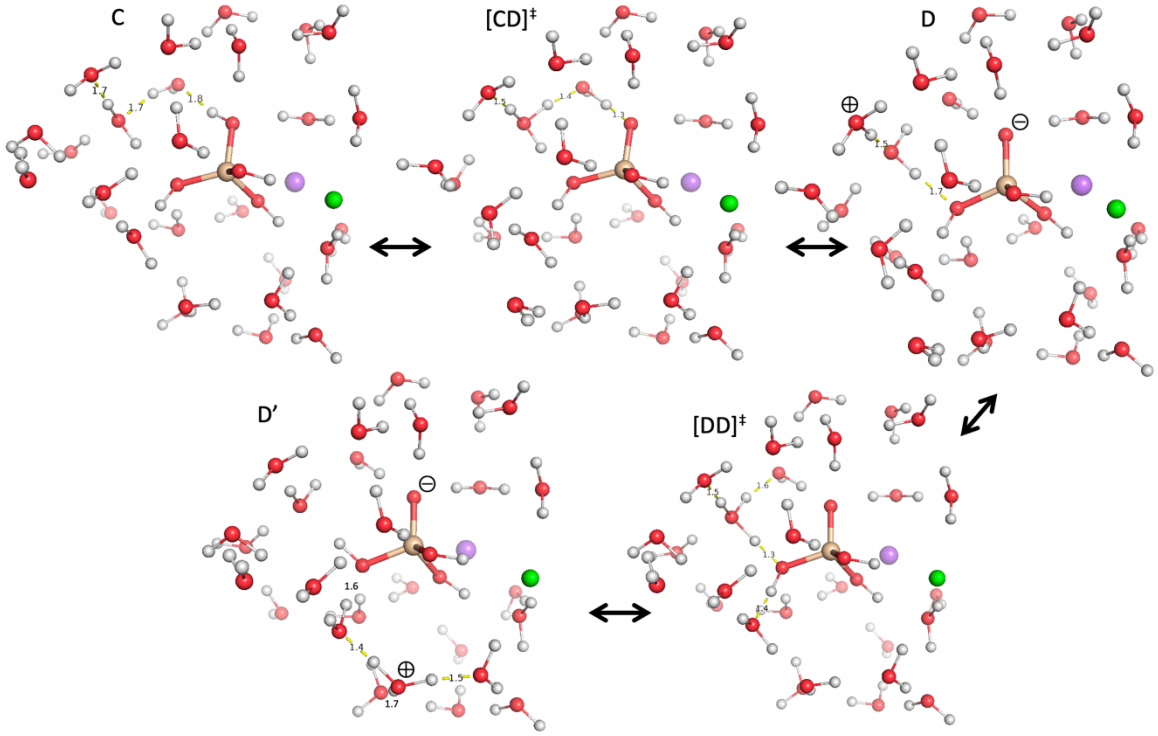

Figure 4. Dimerization in pure water. Mechanism from orthosilicic acid (A) to the dimer (D) optimized with the B3LYP method with customized basis sets. Atoms depicted by ball-and-stick are centers that use the higher level 6-311++G(d,p) basis sets. The rest of the atom centers use 6-31+G(d) basis sets. Corresponding energy changes are shown in Table 2.

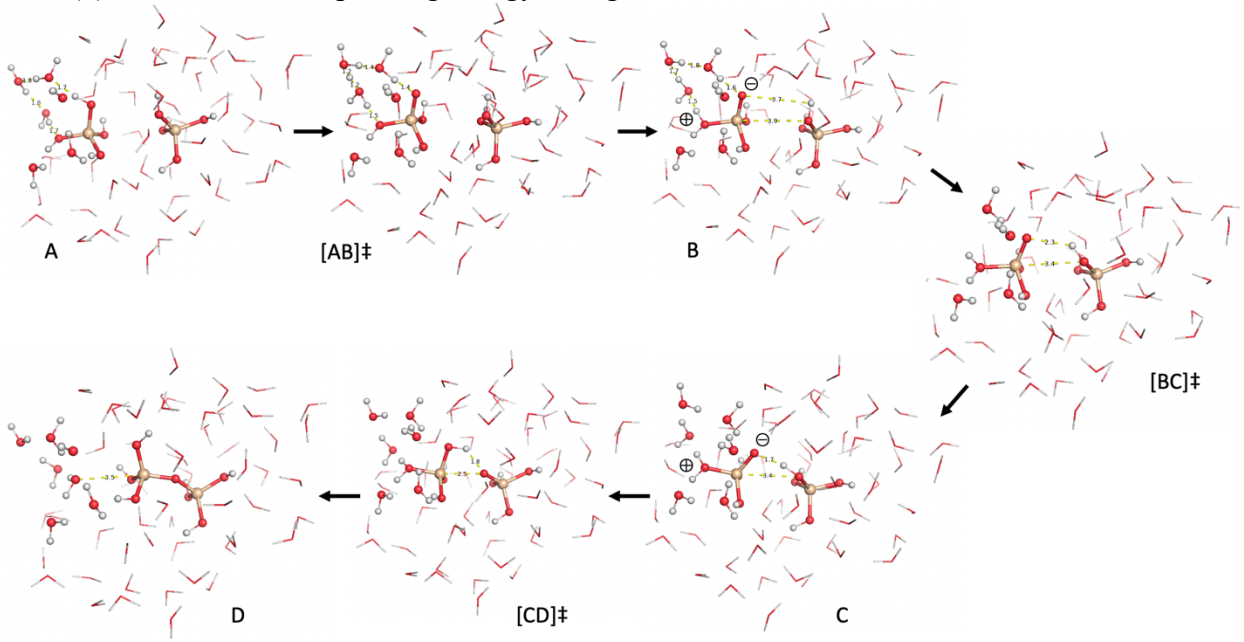

Figure 5. Auto-ionization in pure water. Mechanism from OSAZ (C) to $H_3SiO_4^-$ +H_3O^+ (D) optimized with the B3LYP method. Atoms depicted by ball-and-stick are centers that use the higher level 6-311++G(d,p) basis sets. The rest of the atom centers use 6-31+G(d) basis sets. Corresponding energy changes are shown in Table 2.

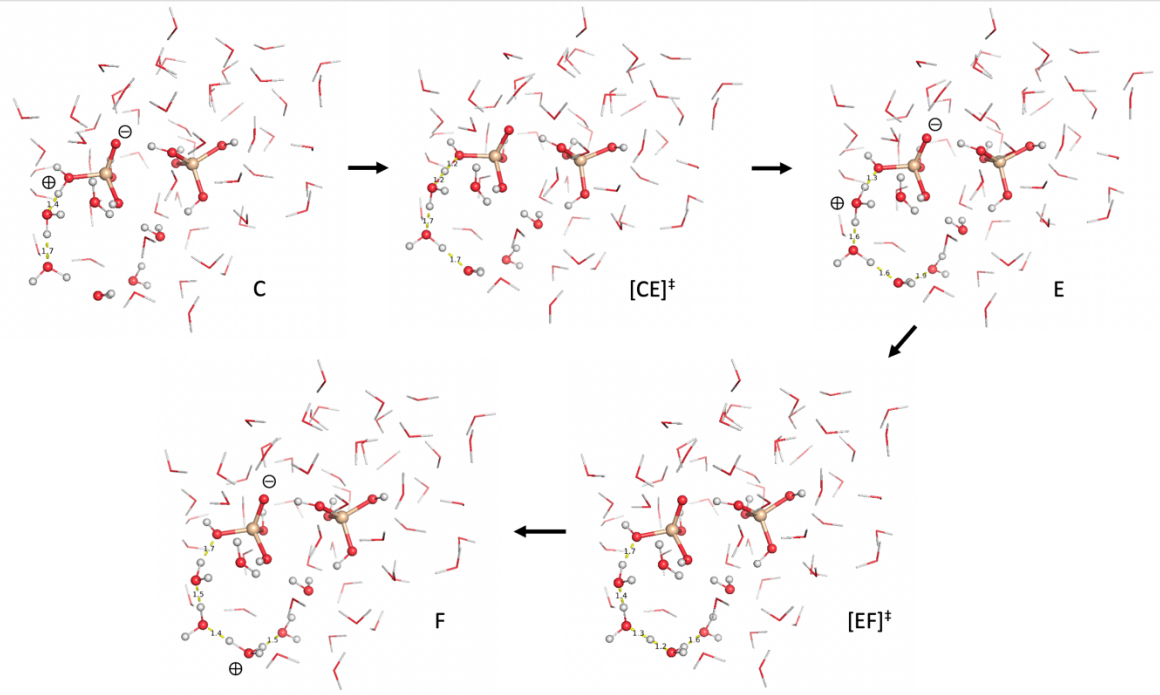

675 Figure 6. Energy Diagram. The letters correspond to configurations in Figure 4 and 5.
676

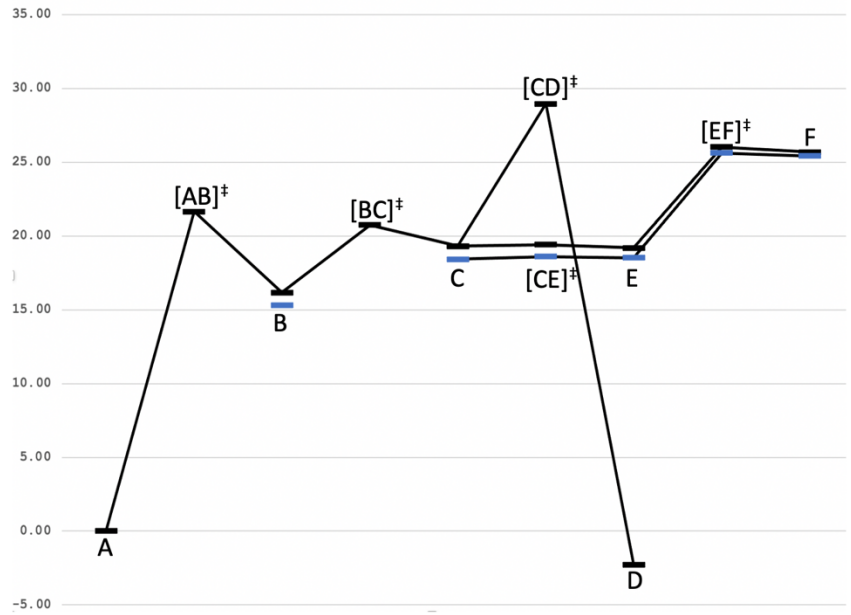

677

Figure 7. Dimerization with NaCl present. Mechanism from orthosilicic acid (G) to the dimer (I) optimized with the B3LYP method with customized basis sets. Atoms depicted by ball-and-stick are centers that use the higher level 6-311++G(d,p) basis sets. The rest of the atom centers use 6-31+G(d) basis sets. Corresponding energy changes are shown in Table 4.

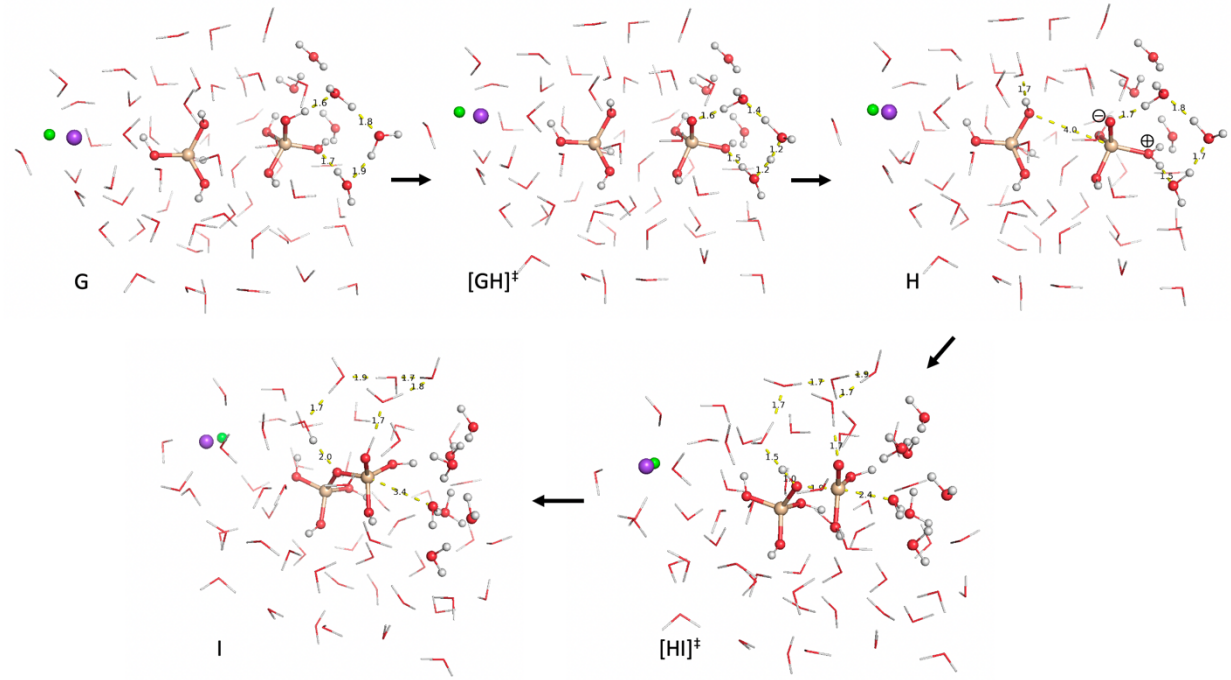

Figure 8. Auto-ionization with NaCl present. Mechanism from OSAZ (H) to $H_3SiO_4^- + H_3O^+$ (J) optimized with the B3LYP method. Atoms depicted by ball-and-stick are centers that use the higher level 6-311++G(d,p) basis sets. The rest of the atom centers use 6-31+G(d) basis sets. Corresponding energy changes are shown in Table 4.

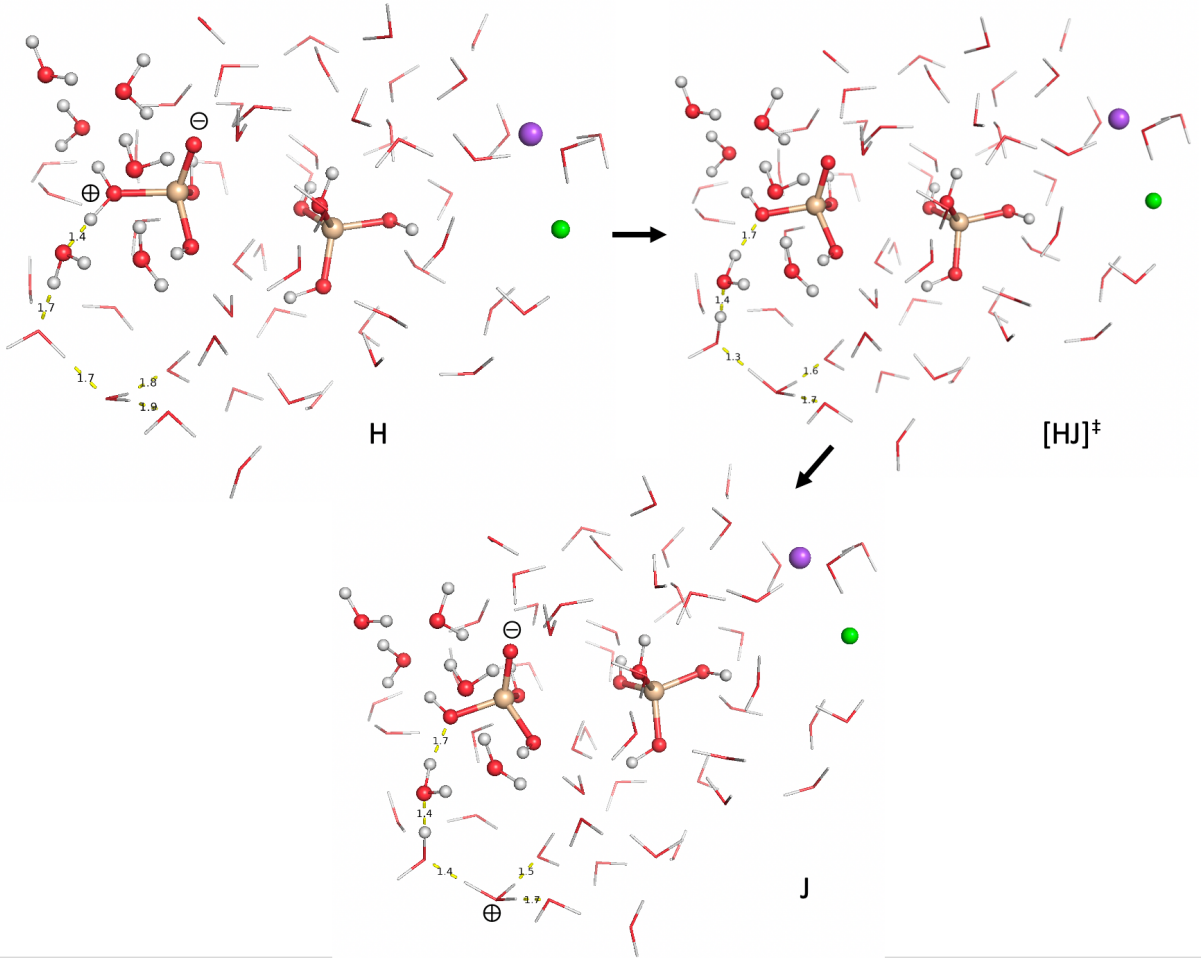

Figure 9. Energy Diagram. The letters correspond to configurations in Figure 7 and 8.